RESEARCH ARTICLE

Monitoring Tumor Targeting and Treatment Effects of IRDye 800CW and GX1-Conjugated Polylactic Acid Nanoparticles Encapsulating Endostar on Glioma by Optical Molecular Imaging

Yaqian Li, Yang Du*, Xia Liu, Qian Zhang, Lijia Jing, Xiaolong Liang, Chongwei Chi, Zhifei Dai, and Jie Tian*

Abstract

Molecular imaging used in cancer diagnosis and therapeutic response monitoring is important for glioblastoma (GBM) research. Antiangiogenic therapy currently is one of the emerging approaches for GBM treatment. In this study, a multifunctional nanoparticle was fabricated that can facilitate the fluorescence imaging of tumor and deliver a therapeutic agent to the tumor region in vivo and therefore possesses broad application in cancer diagnosis and treatment. This particle was polylactic acid (PLA) nanoparticles encapsulating Endostar, which was further conjugated with GX1 peptide and the near-infrared (NIR) dye IRDye 800CW (IGPNE). We demonstrated noninvasive angiogenesis targeting and therapy of IGPNE on U87MG xenografts in vivo using dual-modality optical molecular imaging including NIR fluorescence molecular imaging (FMI) and bioluminescence imaging (BLI). The NIR FMI results demonstrated that IGPNE had more accumulation to the tumor site compared to free IRDye 800CW. To further evaluate the antitumor treatment efficacy of IGPNE, BLI and immunohistochemistry analysis were performed on tumor-bearing mice. With the aid of molecular imaging, the results confirmed that IGPNE enhanced antitumor treatment efficacy compared to free Endostar. In conclusion, IGPNE can realize real-time imaging of U87MG tumors and improve the antiangiogenic therapeutic efficacy in vivo.

1

Introduction

GLIOBLASTOMA (GBM), the most common primary malignant brain tumor in adults, causes neurologic morbidity and remains uniformly fatal. GBM accounts for 12 to 15% of all intracranial tumors and 50 to 60% of astrocytic tumors.[1,2] Currently, the standard of care for GBM is surgery followed by radiation therapy or combined radiotherapy and chemotherapy.[3] Some chemotherapeutic drugs, such as temozolomide and bevacizumab, have been approved by the US Food and Drug Administration for the treatment of adult patients with newly diagnosed GBM.[4,5] Also, there are several trials that involve many types of therapy, including antiangiogenic therapy,[6] viral and gene therapy,[7,8] cancer stem cell therapy,[9] and targeted therapy for treatment of GBM.[10] Despite recent advances in aggressive multimodal treatments, patients with GBM have a dismal prognosis, with a median survival time of less than 15 months.[11] Therefore, new drugs and new delivery systems for targeted therapy and clinically relevant therapy response monitoring for the GBM are urgently needed.

As tremendous development of noninvasive optical molecular imaging technologies for cancer diagnosis and therapeutic response monitoring, in vivo studies of tumors are rapidly becoming an important field for cancer research. The optical molecular imaging presents an attractive option for the visualization and quantification of the cellular and physiologic processes in vivo.[12,13] The ability to detect tumors and measure responses to therapy by imaging technology is a promising field of preclinical and clinical

2

From the School of Automation and Nanomedicine and Biosensor Laboratory, Harbin University of Science and Technology, Haerbin, China; Key Laboratory of Molecular Imaging, Institute of Automation, Chinese Academy of Sciences, Beijing, China; and Department of Biomedical Engineering, College of Engineering, Peking University, Beijing, China.

* *Authors who contributed equally to this work.*

Address reprint requests to: Xia Liu, School of Automation, Harbin University of Science and Technology, 95 XueFu Road, 150080, Harbin, China; e-mail: liuxia@hrbust.edu.cn; or Jie Tian, Key Laboratory of Molecular Imaging, Institute of Automation, Chinese Academy of Sciences, 95 ZhongGuanCun East Road, 100190, Beijing, China; e-mail: jie.tian@ia.ac.cn.

DOI 10.2310/7290.2015.00014

DECKER

research.[14] Furthermore, near-infrared (NIR) light reduced fluorescence background and enhanced tissue penetration, which allows detection of targets located at the depth up to 1 to 2 cm in the tissues.[15,16] The optical probes ICG and IRDye 800CW are favored for use in the NIR region in preclinical and clinical studies.[17,18] Overall, NIR fluorescence molecular imaging (FMI) and bioluminescence imaging (BLI) have significantly contributed to cancer preclinical research and clinical applications, which can evaluate tumor physiologic status in vivo, such as abnormal microenvironments, angiogenesis, metabolism, malignancy, and metastasis.[19,20]

Since the essential role of angiogenesis in tumor formation and metastasis was proposed by Folkman in 1971,[21] increasing attention has been paid to tumor vascular targeted therapy.[22] Microvascular proliferation is a pathologic hallmark of GBM due to the high expression of proangiogenic cytokines.[23] The dependence of tumor growth and metastasis on angiogenesis has been extensively demonstrated in animal models, which provided a powerful rationale for antiangiogenic approaches to cancer therapy. Due to the role of vascular endothelium as a central target for intervention and being less prone to the development of drug resistance, angiogenesis-targeted therapy has become a promising new approach for cancer therapy now.[24,25] The inhibition of tumor growth by antiangiogenic drugs has been achieved in both preclinical studies and clinical trials. As a modified and recombinant human endostatin, Endostar was approved by the State of Food and Drug Administration in China for clinical applications in 2005. Endostar has been investigated clinically combined with the first-line chemotherapy regimen in patients with advanced non–small cell lung cancer and has been demonstrated to inhibit the growth of a variety of human tumors by inhibiting neovascularization and to be superior to other recombinant endostatins.[26,27] Continuous subcutaneous administration of endostatin resulted in inhibiting the growth of U87MG (a human neuronal GBM cell line) tumors in a tumor-bearing mouse model as reported.[25,28,29] However, despite its apparent therapeutic value, the biological half-life of Endostar in vivo is short due to its rapid metabolism, similar to most protein drugs.[30] Therefore, a long-acting and more stable formulation of Endostar is expected.

Delivering drugs specifically to the tumor site and prolonging the half-life of drugs in vivo, which can provide stable antitumor treatment effects, are expected. When conjugated with specific ligands, drugs can accumulate at the target site and improve the detection specificity of tumor and antitumor effects.[31,32] The cancer-specific ligands usually include small molecules, peptides, antibodies, and nanoparticles.[33–36] In particular, low-molecular-weight peptides have satisfactory pharmacokinetics and tissue distribution patterns.[37] As previously reported, the GX1 peptide is a tumor vasculature endothelium-specific ligand. The GX1 peptide, a cyclic 9-mer peptide (CGNSNPKSC), was observed to be bound to human umbilical vein endothelial cells by enzyme-linked immunosorbent assay (ELISA). The specific ability of GX1 peptide to target tumor endothelial cells has been confirmed using different molecular imaging modalities.[38,39] It is evident that GX1 peptide could be a potential candidate for targeted drug delivery in antiangiogenic therapy to improve the diagnosis and therapy of GBM. We used the GX1 peptide as the targeting agent to show its targeting ability and antitumor treatment efficacy in a U87MG tumor–bearing mouse model. To the best of our knowledge, no study on the targeted drug delivery of a combination of Endostar and the GX1 peptide to treat malignant glioma in vivo has been reported.

In this study, we synthesized polylactic acid (PLA) nanoparticles encapsulating Endostar (IGPNE), which was GX1 peptide and NIR dye IRDye 800CW conjugated PLA nanoparticles encapsulating the antiangiogenic drug Endostar, with the aim of improving tumor detection and antiangiogenic therapy against U87MG xenografts in vivo. The surface of the nanoparticles was conjugated with the NIR dye IRDye 800CW to dynamically examine the biodistribution and pharmacokinetics of IGPNE. The tumor accumulation efficiency of IGPNE was evaluated in vivo through NIR FMI based on human U87MG xenografts. Furthermore, the therapeutic efficacy was dynamically monitored not only manually by measuring tumor volumes using digital caliper but also with the use of noninvasive BLI in vivo. Histologic evaluation was also performed at the end of the treatment period for further confirmation of the treatment efficacy of IGPNE in U87MG tumor–bearing mice.

Materials and Methods

Materials and Reagents

Dulbecco's Modified Eagle's Medium (DMEM) was bought from HyClone (Thermo Scientific, Waltham, MA). Minimum Essential Medium with Earle's Balanced Salts and nonessential amino acids (MEM-EBSS) was obtained from MACGENE (Beijing, China). Purified rat antimouse CD31 monoclonal antibody was purchased from BD Biosciences (San Jose, CA). Alexa Fluor 488 donkey antirat lgG was purchased from Invitrogen (USA). Dapi Fluoromount-G was obtained from SouthernBiotech (Birmingham, AL). Endostar was purchased from Shandong Simcere Medgeen Bio-Pharmaceutical Co., Ltd (Nanjing, China). IRDye

800CW was purchased from Li-COR Biosciences (Lincoln, NE). PLA was obtained from Medical Instrumental Institute (Shandong, China). D-Luciferin was purchased from Biotium (Fremont, CA). GX1 peptide (CGNSNPKSC) was synthesized by APeptides Co., Ltd (Shanghai, China).

Synthesis of IGPNE

Endostar was used as a model drug and PLA as a carrying agent to prepare PLA-encapsulating Endostar nanoparticles (PENs) by the water-in-oil-in-water (W/O/W) double emulsion solvent evaporation method.[40] To synthesize PENs, 60 mg of PLA was dissolved in 10 mL of methylene chloride and mixed with the Endostar solution (3 mL, 5 mg/mL). The first emulsion (W/O) was generated by shearing (2,800 rpm for 60 seconds) the mixture. The first W/O
6 emulsion was then poured into a polyvinyl alcohol (PVA) solution (20 mL, 0.1% w/v) and homogenized to obtain the double emulsion (W/O/W) by high-speed shearing (25,000 rpm for 60 seconds). The double W/O/W emulsion was evaporated in 100 mL aqueous solution containing 0.1% PVA (w/v) under gentle magnetic stirring at room temperature until almost all of the methylene chloride evaporated. The PENs were collected by centrifugation (15,300 rpm for 60 minutes), washed three times with phosphate-buffered saline (PBS), and lyophilized (−54°C, 36 hours) by
7 using a freeze dryer (TFD5505, Ilshin Lab, USA).

Three milligrams of IRDye 800CW and 120 μL of EDC/
8 NHS (10 mg/mL) were added to a suspension of the dry PENs in PBS and gently stirred for 24 hours. The PENs-IRDye 800CW was collected by centrifugation with a centrifugal speed of 15,300 rpm for 40 minutes and lyophilized. Then 4 mg of GX1 peptide and 120 μL of EDC/NHS (10 mg/mL) were added into a suspension of the dry PENs-IRDye 800CW in PBS and gently stirred for 24 hours. When the reaction was finished, the product was purified by centrifugation with a centrifugal speed of 15,300 rpm for 40 minutes, washed with PBS three times, and lyophilized at −55°C for 72 hours to obtain the target compound of IGPNE. The IGPNE was stored in the dark at −20°C until use.

Characterization

The size distribution and zeta potential of the nanoparticles were evaluated by a 90Plus/BI-MAS instrument (Brookhaven Instruments Co., Holtvsille, NY). The loading efficiency of Endostar was measured using a Pierce bicinchoninic acid assay (BCA) (Thermo Scientific). The amount of Endostar loaded into the IGPNE was evaluated by detecting the free Endostar during the purification procedure using a Pierce BCA (Thermo Scientific).

Cell Culture

U87MG is a human neuronal GBM cell line that was obtained from the School of Basic Medicine, Peking Union Medical College, Institute of Basic Medical Sciences, Chinese Academy of Medical Sciences. U87MG cells were cultured in MEM-EBSS supplemented with 10% (vol/vol) fetal calf serum (FCS; HyClone, Thermo Scientific). The dual-labeled human GBM cells (U87MG-fLuc-RFP; Shanghai, China), which were transfected with a lentivirus coding for a fusion protein consisting of firefly luciferase according to standard procedures and also expressed red fluorescent protein through gene expression, were cultured in high-glucose DMEM supplemented with 10% (vol/vol) FCS. All cells were maintained at 37°C in a 5% CO2 incubator. No significant differences were observed between U87MG cells and U87MG-fLuc-RFP cells in terms of cell proliferation, migration, and tumorigenicity.

Tumor Model

Five- to 6-week-old athymic male BALB/c nude mice were purchased from the Department of Experimental Animals, Academy of Military Medical Sciences, and were maintained in filtertop cages with free access to food and water in pathogen-free conditions. All animal experiments were performed following the guidelines of the Institutional Animal Care and Use Committee at the Academy of Military Medical Sciences. U87MG-fLuc-RFP cells (1×10^7/100 μL PBS) were subcutaneously injected into the right axillary regions of male BALB/c nude mice to generate the glioma xenograft. The health status of the animals was monitored daily.

In Vivo Biodistribution of IGPNE

To examine the accumulation of IGPNE at the tumor site in vivo, IGPNE was administered to nude mice bearing a subcutaneous U87MG tumor. Specifically, U87MG tumor–bearing mice with tumor volume around 100 μL were randomly divided into two groups: IGPNE and IRDye 800CW (n = 3 mice per group). In vivo biodistribution of IGPNE was assessed using NIR FMI. In vivo study of U87MG tumor–bearing mice was performed to examine the tumor-targeting effects and biodistribution of IGPNE. Male nude mice bearing U87MG xenografts were administered IGPNE (200 μL, 5 mg/mL) via the tail vein, and free IRDye 800CW (200 μL, 5 mg/mL) was used as the control. Before injection, mice were anesthetized and subjected to NIR FMI. The NIR FMI data were collected at 0, 1, 4, 8, 12, and 24 hours postinjection and analyzed by IVIS Living Imaging 3.0 software (PerkinElmer, Waltham, MA). The parameters for NIR FMI of IGPNE were λex = 745 nm, λem = 800 nm, binning = 4, exposure time = 1 second.

NIR FMI signal intensity was assessed quantitatively by comparing the activity in a background (muscle on the same mouse) region of interest (ROI) to the signal intensity from an equal-sized ROI of the tumor. The formulation of NIR FMI light signal to noise ratio (SNR) is as follows:

$$(\mathrm{SNR}) = \frac{\text{Fluorescence light intensity}_{\text{tumor}}}{\text{Fluorescence light intensity}_{\text{muscle}}} \quad \text{(Eq. 1)}$$

Drug Administration

When U87MG-fLuc-RFP tumor–bearing mice with, tumor volume reached an average size of 100 μL. The mice were randomly divided into three groups (n = 5 mice per group), including PBS (control), Endostar (10 mg/kg), and IGPNE (10 mg/kg). The agents were administrated via tail vein injection every day for 15 consecutive days. The control group was given an equal volume of PBS in parallel for comparison.

Mouse Body Weight Measurement and Tumor Volume Calculation

The tumor volume and mouse body weight in each group (n = 5) were measured every 3 days until day 15. Tumor volume was determined by digital caliper by measuring the length (L) and width (W), and the tumor volume was calculated according to the formula $\pi \times \mathrm{L} \times \mathrm{W}^2/6$. The tumor volume inhibition was calculated according to the following equation:

$$\text{Tumor volume inhibition} = \left(1 - \frac{\text{Volume}_{\text{Day0 experiment group}} - \text{Volume}_{\text{DayN experiment group}}}{\text{Volume}_{\text{Day0 control group}} - \text{Volume}_{\text{DayN control group}}}\right) \times 100\% \quad \text{(Eq. 2)}$$

In Vivo BLI of Subcutaneous U87MG Tumor Xenografts

To evaluate the therapeutic effects of Endostar and IGPNE for GBM in vivo, BLI was implemented to the subcutaneous U87MG tumor mouse model by using a small animal optical molecular imaging system (IVIS Imaging Spectrum System, Caliper Life Sciences, USA) on days 0, 3, 6, 9, 12, and 15 during drug treatment. Twelve hours before the experiment, the mice were fasted to prevent food from interfering with the imaging results. BLIs of the mice were acquired 10 minutes after intraperitoneal injection of 80 μL (15 mg/mL) of D-luciferin solution. The mice were anesthetized by gas anesthesia and then were placed into the imaging system in the lateral position. The parameters for the BLI system were binning = 4 and exposure time = 1 second. BLI signal intensity was quantitatively assessed by measuring the signal intensity from an equal-sized ROI of the tumors from tumor-bearing mice in the control, Endostar, and IGPNE groups through Living Image 4.4 software (IVIS Imaging Spectrum System, Caliper).

Histopathology and CD31 Immunohistochemistry

The mice were sacrificed and tumors were harvested after a 15-day treatment period. The tumors were frozen in the optimum cutting temperature (OCT) compound (Leica, Wetzlar, Germany) for cryosections. Frozen U87MG tumor tissues were cryosectioned at 8 μm thick by Cryostat Microtome (CM1950, Leica) and evaluated by standard hematoxylin-eosin (H&E) staining and immunohistochemistry (IHC). IHC was performed using rat antimouse CD31 antibody and Alexa Fluor 488 donkey antirat lgG. Briefly, frozen U87MG tumor tissue slices were fixed in acetone for 10 minutes and then washed in PBS. The slides were incubated with primary antibodies of rat antimouse CD31 antibodies at 4°C overnight, rinsed in PBS, and incubated with secondary antibodies of Alexa Fluor 488 donkey antirat lgG. Tumor tissue sections that were stained with Alexa Fluor 488 donkey antirat lgG only were used as a negative control. After washing three times with PBS and nuclear staining with DAPI, sections were mounted and analyzed under inverted fluorescence microscopy (Leica Microsystems AG). The CD31 fluorescence light intensity was semiquantified using Leica AF software.

Statistical Analysis

All results were presented as a mean of three independent experiments (mean ± SEM). One-way analysis of variance (ANOVA) or Student t-test was performed to compare the statistical differences. Analyses were performed using GraphPad Prism software version 5.0 (San Diego, CA), and p values $< .05 < .01$, and $< .001$were considered statistically significant.

Results

Characterization of the Nanoparticles

The characteristics of the blank PLA nanoparticles and IGPNE were analyzed. DLS results revealed that the PLA nanoparticles showed a mean diameter of 93.7 ± 12.6 nm. The zeta potential of the PLA nanoparticles was evaluated as −25 ± 1.8 mV. After loading with Endostar, the diameter of the IGPNE was increased, with a mean diameter of 104.3 ± 15.6 nm, and the zeta potential was evaluated as −22 ± 3.5 mV. By using the Pierce BCA (Thermo Scientific), the encapsulation efficiency of Endostar was 75.8 ± 6.6%, and the loading content of Endostar in our agent was 2.7 ± 0.6%.

Monitoring the Biodistribution of IGPNE In Vivo Using NIR FMI

To evaluate the tumor accumulation efficiency of IGPNE, NIR FMI was acquired after intravenous injection of IGPNE into U87MG xenograft mouse models, and free IRDye 800CW was used as the control. Fluorescence signal of IGPNE was significantly accumulated at the tumor site 8 hours after intravenous injection and increased for 24 hours (Figure 1A). The accumulation of IGPNE at the tumor site reached a maximum accumulation at 12 to 24 hours. However, there was no specific increase in signal for the free IRDye 800CW specifically at the tumor site during the whole 24-hour observation. Compared to the free IRDye 800CW group, IGPNE showed a significantly higher signal to noise ratio at the tumor site (Figure 1B). The results suggest that IGPNE is a potential targeted and long-acting formulation of Endostar that may contribute to enhanced antiangiogenesis therapy of GBM.

Mouse Body Weight and Tumor Volume Changes after Different Drug Treatment

The growth of tumor nodules was measured using a digital caliper during the 15-day drug treatment. In the control group, tumor nodules gradually grew during the experimental time course. Endostar and IGPNE treatments could slow down the growth of tumors, and IGPNE exhibited more significant inhibition of tumor growth than Endostar (Figure 2A). In terms of tumor volume inhibition, IGPNE exhibited more enhanced tumor growth suppression than free Endostar (Figure 2B). On day 15, the tumor volume inhibition of IGPNE reached 80.83 ± 5.94%; however, the tumor volume inhibition of Endostar was 60.02 ± 4.52%. The data suggest that targeted treatment of IGPNE increases the antitumor effect of Endostar.

Mouse body weight was also monitored during the drug treatment period (Figure 2C). The results show that both Endostar and IGPNE treatment did not lead to body weight loss during drug treatment compared to the control group. Thus, both Endostar and IGPNE treatment are relatively safe, with no serious side effects.

Monitoring Tumor Growth with Different Drug Treatment through BLI In Vivo

BLI was performed using the small animal optical molecular imaging system on days 0, 3, 6, 9, 12, and 15 during drug treatment, and the antitumor treatment efficacy of free

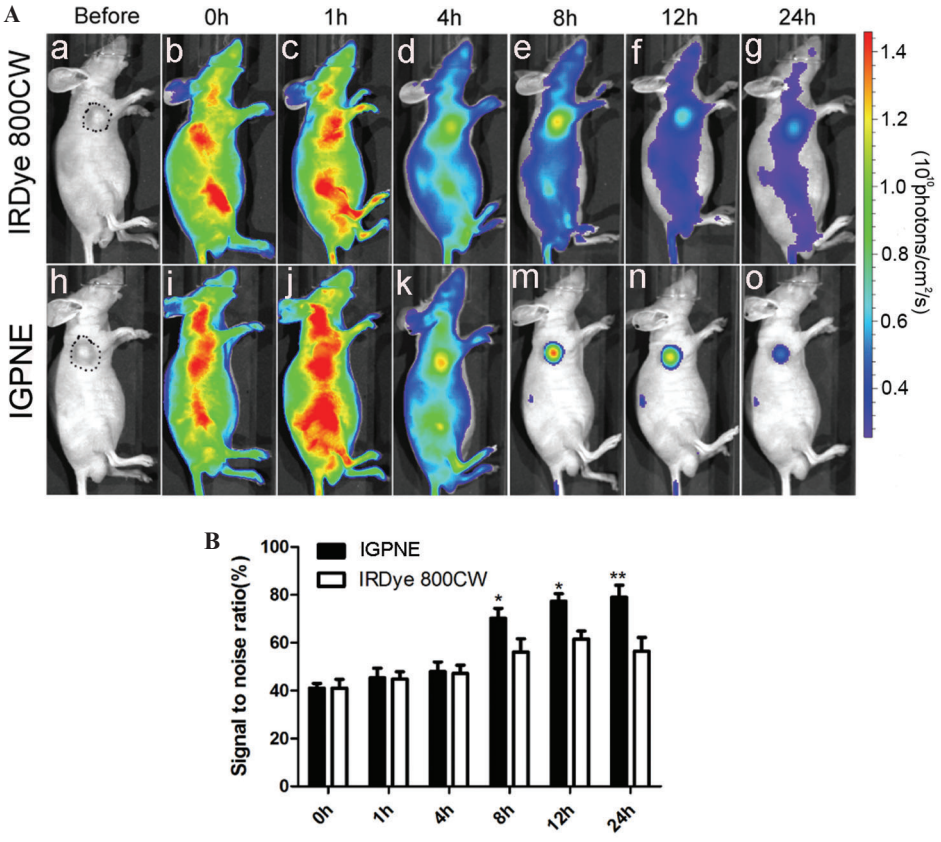

Figure 1. The biodistribution of IGPNE in vivo monitored through near-infrared fluorescence molecular imaging (NIR FMI). *A*, The tumor sites are delineated with a *black dotted line* (a and h). The biodistribution of free IRDye 800CW (b–g) and IGPNE (i–o) in the tumor-bearing nude mice was monitored through NIR FMI for 24 hours. *B*, The NIR FMI light signal to noise ratio (SNR) of IGPNE and free IRDye 800CW in vivo. $^{*}p < .05$; $^{**}p < .01$.

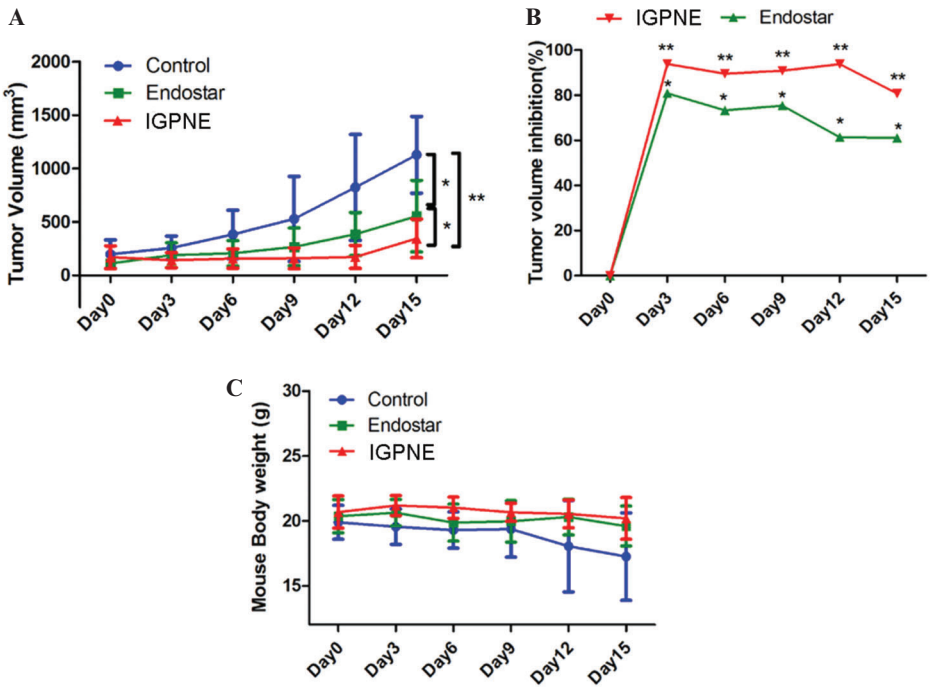

Figure 2. The mouse body weight and tumor volume changes during continuous drug treatment for 15 days. The average mouse tumor volume (A), tumor volume inhibition (B), and average mouse body weight (C) treated with control, Endostar, and IGPNE. The data are presented as mean ± standard error of the mean. $^{*}p < .05$; $^{**}p < .01$.

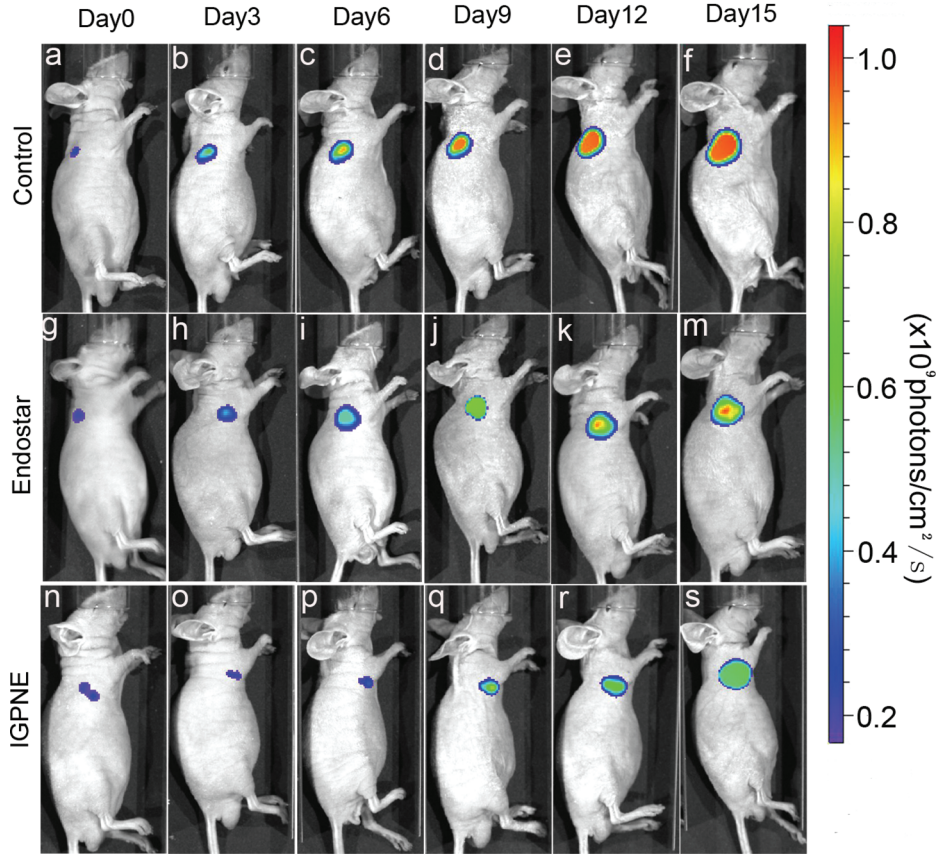

Figure 3. The representative bioluminescence imaging (BLI) of tumors with different continuous treatments for 15 days. With the aid of labeled fLuc, the nude mice bearing U87MG tumors derived from U87MG-fLuc-RFP cells displayed BLI, the signal intensities of which reflected the drug's treatment efficacy in vivo. The BLI of U87MG tumors with different treatments included the control group (a–f), Endostar treatment (g–m), and IGPNE treatment (n–s).

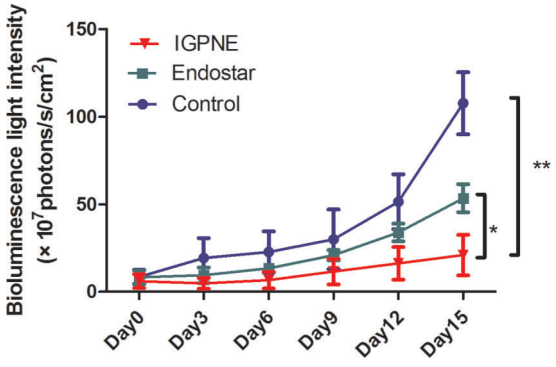

Figure 4. Bioluminescence imaging intensity for tumor-bearing mice in the control, Endostar, and IGPNE groups during the 15-day observation. The data are presented as mean ± standard error of the mean. $^{*}p < .05$; $^{**}p < .01$.

Endostar and IGPNE was assessed quantitatively by comparing the BLI signal intensity. The light signals in the control group increased steadily during the whole treatment period (Figure 3, a–f). Endostar (Figure 3, g–m) treatment did slow the increase in light signal of tumors compared to the control groups (see Figure 3, a–f). IGPNE (Figure 3, n–s) exhibited the most significant inhibition of light signal increase compared to the free Endostar group. The BLI light intensity in the control group was 107.6 ± 15.704 × 107 p/cm^2/s, and the BLI light intensity in the Endostar-treated group was 53.40 ± 8.02 × 107 p/cm^2/s on day 15. The BLI intensity in the IGPNE-treated group was only 20.97 ± 9.34 × 107 p/cm^2/s (Figure 4). Consistent with the data in Figure 2A, IGPNE showed enhanced tumor growth suppression effect compared to the free Endostar treatment. The data support the prominent and safe antitumor efficacy of IGPNE in vivo.

Immunohistologic Examination of the Effects of IGPNE on Tumor Angiogenesis

CD31 staining and H&E histology were performed to validate the therapeutic efficacy of free Endostar and IGPNE treatment. CD31 is the biomarker of microvessels. The CD31 fluorescence light intensity was 912.907 ± 19.115 in the control group and 570.018 ± 4.751 in the Endostar-treated group. The CD31 fluorescence light intensity in the IGPNE-treated group was only 398.074 ± 11.893 (Figure 5 and Figure 6). Consistent with the in vivo BLI data, the CD31 expression level was highest in the control group, and the CD31-positive microvessels in the IGPNE treatment group were much less than in the other two groups. H&E staining of U87MG xenograft was also performed. It was found that Endostar and IGPNE exhibited fewer tumor cells compared to the control group, and the IGPNE treatment group had fewer tumor cells than the Endostar group (see Figure 5, h and l). The results indicate that IGPNE successfully improved the tumor angiogenic inhibition efficacy for GBM compared to the other two groups, as well as improved the tumor cell growth inhibition of Endostar.

Discussion

In this work, we developed novel IRDye800CW and GX1-conjugated PLA nanoparticles encapsulating Endostar, which, with the aid of molecular imaging, can be used for improving tumor detection and antiangiogenic therapy against U87MG glioma xenografts in vivo.

As the development of molecular imaging technologies exists for the diagnosis of cancer and monitoring the therapeutic response, optical molecular imaging is especially appealing because of its low cost, high sensitivity, and spatial resolution and absence of ionizing radiation.[41] Moreover, NIR light reduced fluorescence background and enhanced tissue penetration. NIR FMI and BLI are already the modalities of choice for preclinical studies.[14]

To improve therapeutic indices and to deliver drugs to the tumor site efficiently, more specific and selective anticancer agents that can discriminate between tumor and nonmalignant cells are urgently needed. Antiangiogenic therapy could be improved by coupling it with molecular markers specifically targeting tumor blood vessels.[42] A new tumor-homing peptide motif, GX1, which was recorded specifically binding to human umbilical vein endothelial cells, was identified using in vivo selection of phage display libraries.[15,39] The polymer system PLA was approved by the US Food and Drug Administration and used in this study as a nanocarrier for drug loading against malignant glioma.[43] Additionally, the PLA system was chosen as it can incorporate a variety of compounds within the polymer on forming nanoparticles. Endostar, as an endogenous inhibitor of angiogenesis, has been verified to combine with standard chemotherapy regimens to improve tumor regression. It has been reported that Endostar successfully improved the inhibition of the U87MG xenograft tumor growth when combined with targeted radiotherapy.[25,30] Tumor growth was significantly inhibited only by administering Endostar via peritumoral subcutaneous injection, possibly due to the poor concentration of Endostar dose in U87MG tumor by systemic administration, which was also proved by Schmidt and colleagues.[44] Therefore, in this study, we used the angiogenesis-targeting peptide GX1 and the NIR fluorescent dye IRDye 800CW conjugated with the PLA nanosystem encapsulating Endostar and investigated

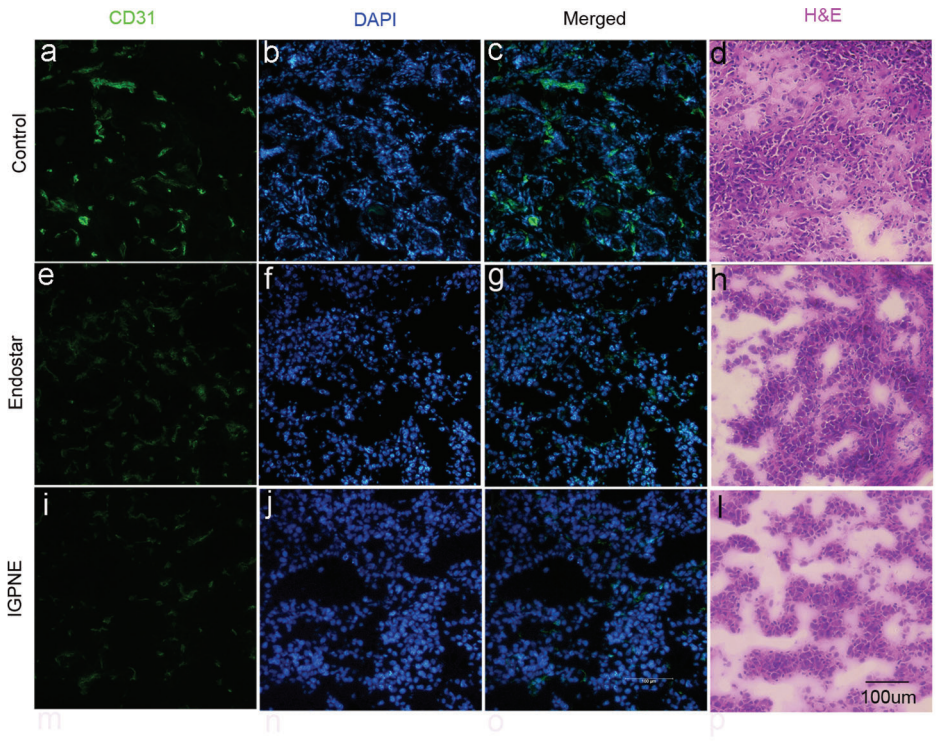

Figure 5. CD31 and hematoxylin-eosin (H&E) staining of tumor sections from mice treated continuously over 15 days. CD31 is a microvascular marker, and CD31 staining was used to evaluate the antiangiogenic effects of various drug treatments. CD31 expression is shown in *green* (a, e, i); the nuclei were stained with DAPI in *blue* (b, f, j); merged CD31 and DAPI images (c, g, k). The H&E histology of tumor tissues is shown (d, h, l) (scale bar = 100 μm, 20×).

its biodistribution, tumor-targeting effects, and antitumor treatment efficacy.

With the labeling of NIR dye IRDye 800CW, the biodistribution and tumor-accumulating effects of IGPNE can be monitored in vivo using NIR FMI (see Figure 1A). The NIR FMI of IGPNE in U87MG tumors revealed high tumor uptake and fast clearance from nontargeted organs compared to free IRDye 800CW. The results suggest that the GX1 peptide facilitated Endostar accumulation at the tumor regions and that IGPNE acquired the capability of controlled drug release specifically at tumor sites. In particular, with the advantage of the relatively long half-life of IGPNE, very high and potentially tumoricidal accumulated absorbed doses and good therapeutic efficacy could be achieved.

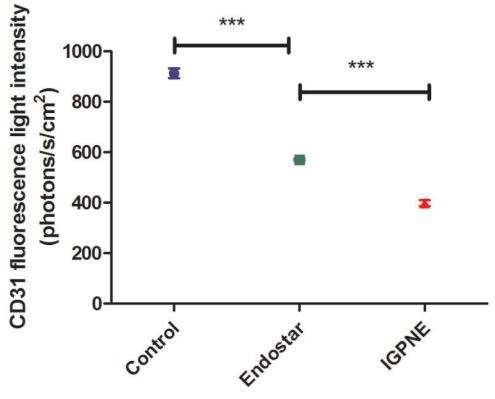

Figure 6. CD31 fluorescence light intensity of the tumor sections in the control, Endostar, and IGPNE groups after the 15-day treatment period. The data are presented as mean ± standard error of the mean. *** $p < .001$.

After monitoring the biodistribution of the IGPNE in vivo, the antitumor treatment efficacy against GBM of IGPNE was performed on subcutaneous U87MG tumor–bearing mouse models. The therapeutic efficacy was dynamically monitored not only manually by measuring tumor volumes using a digital caliper (see Figure 2A) but also with the use of BLI (see Figure 3). BLI provided a quantitative surrogate measurement of the number of living tumor cells because the BLI signal was emitted from living tumor cells.[45,46] Real-time BLI of U87MG-fLuc-RFP tumor–bearing mice revealed the inhibition of tumor growth following treatment with free Endostar as well as IGPNE, and the inhibitory effect on tumor growth for IGPNE was more significant than free Endostar. The data suggest an enhanced antitumor effect of IGPNE due to targeted delivery of an antiangiogenic drug so as to achieve inhibition of tumor angiogenesis.

To further confirm the ability of Endostar and IGPNE in therapy for GBM, H&E and CD31 immunostaining were performed. As shown in Figure 5, the results showed the least CD31-positive staining in the IGPNE treatment group compared to the control and free Endostar treatment groups. H&E histologic analysis confirmed that IGPNE had

improved antitumor treatment efficacy compared to free Endostar, which indicated that IGPNE facilitated Endostar accumulation and long-acting at the tumor region.

Conclusion

We developed a novel theranostic nanoparticle, IGPNE, that can be used for the targeted imaging and treatment of the malignant glioma in vivo. IGPNE exhibited improved tumor targeting and antitumor treatment efficacy compared to free Endostar. IGPNE also fulfilled a novel theranostic purpose owing to targeting peptide GX1 facilitated Endostar accumulation specifically at the tumor regions. Our findings may be useful toward the development of a novel treatment regimen in the preclinical setting and application of targeted imaging. In the future, more preclinical studies with IGPNE are needed to determine whether IGPNE would be suitable for clinical application for the treatment of GBM. Other integrin CD31–positive tumor models and an orthotropic tumor model should be involved in further investigations.

Acknowledgment

Financial disclosure of authors: This work was supported by the National Basic Research Program of China (973) (under grants 2015CB755500, 2014CB748600, and 2011CB707702), National Natural Science Foundation of China (81470083, 81227901), Natural Science Foundation of Heilongjiang Province of China (under grant no. F201311), Foundation of Heilongjiang Educational Committee (under grant no. 12541105), and Foundation of Heilongjiang Educational Committee (under grant no. 12531119). The funders had no role in the study design, data collection and analysis, decision to publish, or preparation of the manuscript.

Financial disclosure of reviewers: None reported.

References

1. Furnari FB, Fenton T, Bachoo RM, et al. Malignant astrocytic glioma: genetics, biology, and paths to treatment. Genes Dev 2007;21:2683–710.
2. Buckner JC. Factors influencing survival in high-grade gliomas. Semin Oncol 2003;30:10–4.
3. Siegel R, Naishadham D, Jemal A. Cancer statistics, 2012. CA Cancer J Clin 2012;62:10–29.
4. Stupp R, Mason WP, van den Bent MJ, et al. Radiotherapy plus concomitant and adjuvant temozolomide for glioblastoma. N Engl J Med 2005;352:987–96.
5. de Groot JF, Fuller G, Kumar AJ, et al. Tumor invasion after treatment of glioblastoma with bevacizumab: radiographic and pathologic correlation in humans and mice. Neuro Oncol 2010; 12:233–42.
6. Van Meir EG, Hadjipanayis CG, Norden AD, et al. Exciting new advances in neuro-oncology: the avenue to a cure for malignant glioma. CA Cancer J Clin 2010;60:166–93.
7. Jensen SA, Calvert AE, Volpert G, et al. Bcl2L13 is a ceramide synthase inhibitor in glioblastoma. Proc Natl Acad Sci U S A 2014;111:5682–7.
8. Zhao F, Tian J, An L, et al. Prognostic utility of gene therapy with herpes simplex virus thymidine kinase for patients with high-grade malignant gliomas: a systematic review and meta analysis. J Neurooncol 2014;118:239–46.
9. Li Y, Raman I, Du Y, et al. Kallikrein transduced mesenchymal stem cells protect against anti-GBM disease and lupus nephritis by ameliorating inflammation and oxidative stress. PloS One 2013;8:e67790.
10. Abdullah JM, Mustafa Z, Ideris A. Newcastle disease virus interaction in targeted therapy against proliferation and invasion pathways of glioblastoma multiforme. Biomed Res Int 2014; 2014:386470.
11. Stupp R, Hegi ME, Mason WP, et al. Effects of radiotherapy with concomitant and adjuvant temozolomide versus radiotherapy alone on survival in glioblastoma in a randomised phase III study: 5-year analysis of the EORTC-NCIC trial. Lancet Oncol 2009;10:459–66.
12. Weissleder R. Molecular imaging in cancer. Science 2006;312: 1168–71.
13. Hsu AR, Chen X. Advances in anatomic, functional, and molecular imaging of angiogenesis. J Nucl Med 2008;49:511–4.
14. Belhocine T, Steinmetz N, Green A, et al. In vivo imaging of chemotherapy-induced apoptosis in human cancers. Ann N Y Acad Sci 2003;1010:525–9.
15. Chen K, Yap LP, Park R, et al. A Cy5.5-labeled phage-displayed peptide probe for near-infrared fluorescence imaging of tumor vasculature in living mice. Amino Acids 2012;42:1329–37.
16. Zhu D, Larin KV, Luo Q, et al. Recent progress in tissue optical clearing. Laser Photon Rev 2013;7:732–7.
17. Quan B, Choi K, Kim YH, et al. Near infrared dye indocyanine green doped silica nanoparticles for biological imaging. Talanta 2012;99:387–93.
18. Huang R, Vider J, Kovar JL, et al. Integrin alphavbeta3-targeted IRDye 800CW near-infrared imaging of glioblastoma. Clin Cancer Res 2012;18:5731–40.
19. Hsu AR, Chen X. Advances in anatomic, functional, and molecular imaging of angiogenesis. J Nucl Med 2008;49:511–4.
20. Glunde K, Pathak AP, Bhujwalla ZM. Molecular–functional imaging of cancer: to image and imagine. Trends Mol Med 2007;13:287–97.
21. Folkman J. Tumor angiogenesis: therapeutic implications. N Engl J Med 1971;285:1182–6.
22. Robles Irizarry L, Hambardzumyan D, Nakano I, et al. Therapeutic targeting of VEGF in the treatment of glioblastoma. Expert Opin Ther Targets 2012;16:973–84.
23. Louis DN, Ohgaki H, Wiestler OD, et al. The 2007 WHO classification of tumours of the central nervous system. Acta Neuropathol 2007;114:97–109.
24. Folkman J. Antiangiogenesis in cancer therapy—endostatin and its mechanisms of action. Exp Cell Res 2006;312:594–607.
25. Shi J, Fan D, Dong C, et al. Anti-tumor effect of integrin targeted (177)Lu-3PRGD2 and combined therapy with Endostar. Theranostics 2014;4:256–66.
26. Jiang L, Miao Z, Liu H, et al. 177Lu-labeled RGD-BBN heterodimeric peptide for targeting prostate carcinoma. Nucl Med Commun 2013;34:909–14.

27. Ling Y, Yang Y, Lu N, et al. Endostar, a novel recombinant human endostatin, exerts antiangiogenic effect via blocking VEGF-induced tyrosine phosphorylation of KDR/Flk-1 of endothelial cells. Biochem Biophys Res Commun 2007;361:79–84.
28. Ke QH, Zhou SQ, Huang M, et al. Early efficacy of Endostar combined with chemoradiotherapy for advanced cervical cancers. Asian Pac J Cancer Prev 2012;13:923–6.
29. Li XQ, Shang BY, Wang DC, et al. Endostar, a modified recombinant human endostatin, exhibits synergistic effects with dexamethasone on angiogenesis and hepatoma growth. Cancer Lett 2011;301:212–20.
30. Tong Y, Zhong K, Tian H, et al. Characterization of a monoPEG20000-Endostar. Int J Biol Macromol 2010;46:331–6.
31. Lee S, Xie J, Chen X. Activatable molecular probes for cancer imaging. Curr Top Med Chem 2010;10:1135–44.
32. Hadjipanayis CG, Machaidze R, Kaluzova M, et al. EGFRvIII antibody-conjugated iron oxide nanoparticles for magnetic resonance imaging-guided convection-enhanced delivery and targeted therapy of glioblastoma. Cancer Res 2010;70:6303–12.
33. Lee S, Xie J, Chen X. Peptide-based probes for targeted molecular imaging. Biochemistry 2010;49:1364–76.
34. Ogawa M, Regino CA, Seidel J, et al. Dual-modality molecular imaging using antibodies labeled with activatable fluorescence and a radionuclide for specific and quantitative targeted cancer detection. Bioconjug Chem 2009;20:2177–84.
35. Yu MK, Park J, Jon S. Targeting strategies for multifunctional nanoparticles in cancer imaging and therapy. Theranostics 2012;2:3.
36. Gao J, Chen K, Miao Z, et al. Affibody-based nanoprobes for HER2-expressing cell and tumor imaging. Biomaterials 2011;32: 2141–8.
37. Chen K, Chen X. Design and development of molecular imaging probes. Curr Top Med Chem 2010;10:1227.
38. Hui X, Han Y, Liang S, et al. Specific targeting of the vasculature of gastric cancer by a new tumor-homing peptide CGNSNPKSC. J Control Release 2008;131:86–93.
39. Zhi M, Wu K-C, Dong L, et al. Research paper characterization of a specific phage-displayed peptide binding to vasculature of human gastric cancer. Cancer Biol Ther 2004;3:1232–5.
40. Ke H, Wang J, Dai Z, et al. Gold-nanoshelled microcapsules: a theranostic agent for ultrasound contrast imaging and photothermal therapy. Angew Chem Int Ed Engl 2011;50:3017–21.
41. Kiessling F, Fokong S, Bzyl J, et al. Recent advances in molecular, multimodal and theranostic ultrasound imaging. Adv Drug Deliv Rev 2014;72:15–27.
42. Kolonin M, Pasqualini R, Arap W. Molecular addresses in blood vessels as targets for therapy. Curr Opin Chem Biol 2001;5:308–13.
43. Zhan C, Wei X, Qian J, et al. Co-delivery of TRAIL gene enhances the anti-glioblastoma effect of paclitaxel in vitro and in vivo. J Control Release 2012;160:630–6.
44. Schmidt NO, Ziu M, Carrabba G, et al. Antiangiogenic therapy by local intracerebral microinfusion improves treatment efficiency and survival in an orthotopic human glioblastoma model. Clin Cancer Res 2004;10:1255–62.
45. Ma X, Liu Z, Yang X, et al. Dual-modality monitoring of tumor response to cyclophosphamide therapy in mice with bioluminescence imaging and small-animal positron emission tomography. Mol Imaging 2011;10:278–83.
46. Rehemtulla A, Stegman LD, Cardozo SJ, et al. Rapid and quantitative assessment of cancer treatment response using in vivo bioluminescence imaging. Neoplasia 2000;2:491–5.

Authors Queries

Journal: **Molecular Imaging**
Paper: **MI-2015-01-0002**
Title: **Monitoring Tumor Targeting and Treatment Effects of IRDye 800CW and GX1-Conjugated Polylactic Acid Nanoparticles Encapsulating Endostar on Glioma by Optical Molecular Imaging**

Dear Author
During the preparation of your manuscript for publication, the questions listed below have arisen. Please attend to these matters and return this form with your proof. Many thanks for your assistance

Query Reference	Query	Remarks
1	AU: Can realize? Is the verb correct?	
2	AU: What about the tremendous development? The thought is incomplete. Please advise.	
3	AU: Please spell out ICG if possible.	
4	AU: Not sure if the word you want in these two sentences is "expected." Please confirm.	
5	AU: Please provide the city and state for Invitrogen.	
6	AU: Assumed that PVA = polyvinyl alcohol. If not, please advise.	
7	AU: Please provide the city and state for Ilshin Lab.	
8	AU: Please spell out EDC/NHS.	
9	AU: "When U87MG-fLuc-RFP tumor–bearing mice with" what? Please complete the thought.	

10	AU: Please provide the city and state for Caliper Life Sciences.	
11	AU: Above you just have Leica, so please confirm the company name and make it consistent.	
12	AU: What is DLS? Please spell out.	
13	AU: The number of CD31-positive vessels was much less? Please clarify.	
14	AU: Not sure what you mean by the development of these technologies existing. Please clarify.	
15	AU: The efficacy was performed? Please clarify what you meant here.	
16	AU: Please clarify what you mean by facilitated long acting.	
17	AU: I don't know what you mean here: "fulfilled a novel theranostic purpose owing to targeting peptide GX1 facilitated Endostar accumulation." It doesn't make sense. Please advise.	
18	AU: Please confirm that the disclosure is complete and correct.	